Desalination and Water Treatment
www.deswater.com

doi: 10.5004/dwt.2020.25697

190 (2020) 340–352
June

Removal of EBT dye from aqueous solution by modified $MoNiO_4$ adsorbent

Farhad Salimi[a,*], Vahid Valiei[a], Changiz Karami[b]

[a]*Department of chemical engineering, Kermanshah Branch, Islamic Azad University, Kermanshah, Iran, emails: f.salimi@iauksh.ac.ir (F. Salimi), vahidvalaie90@gmail.com (V. Valaie)*
[b]*Nano Drug Delivery Research Center, Kermanshah University of Medical Sciences, Kermanshah, Iran, email: changiz.karami@gmail.com (C. Karami)*

Received 25 May 2019; Accepted 16 February 2020

ABSTRACT

In this study, the perovskite structures of $MoNiO_4$ (MNO) and modified $MoNiO_4$ (MMNO) nanoparticles were synthesized and used to remove a textile dye, Eriochrome Black T (EBT), from water solution. The MMNO structure was synthesized using the citrate sol–gel method. The Fourier-transform infrared spectroscopy, scanning electronic microscopy analysis, pore size distribution analysis, the N_2 adsorption (Brunauer–Emmett–Teller (BET) specific surface area) analysis, and X-ray diffraction spectroscopy were used to characterize the prepared nanoparticles. The BET results showed that the surface area for MMNO nanoparticle increased slightly with the citrate sol–gel method. The effect of operating parameters such as adsorbent dosage, pH, and contact time were investigated. The maximum adsorption of EBT was obtained as 6.66 and 68.03 mg/g for MNO and MMNO, respectively. The optimum conditions were pH of 7, mixing time of 25 min, the temperature of 25°C, and 5 g/L MNO and MMNO for 100 mg/L EBT solution. The adsorption isotherm and the kinetic study showed that the adsorption EBT on adsorbents (i.e., MNO and MMNO) obeyed Langmuir isotherm and pseudo-second-order model, respectively. Moreover, measuring the thermodynamic parameters revealed that the adsorption process was non-spontaneous and endothermic.

Keywords: Adsorption; $MoNiO_4$ perovskite; Eriochrome Black T; Adsorption behavior

1. Introduction

Annually, about one million tons of dyes are produced in the world's market, of which 70% belongs to azo dyes as the largest class of the commercial dyes [1]. A reactive azo dye contains one or more azo bonds (–N=N–) that act as chromophores in the molecular structure [2]. Also, as the largest group of organic dyes, azo dyes are difficult to degrade even at low concentrations due to its high resistance to light, heat, water, and chemical and microbial attack [3]. Therefore, it is highly essential to remove azo dyes from wastewater effluents before discharge into water bodies.

Many techniques have been introduced to remove dyes from wastewaters. Biological, oxidation, or ozonation [4,5], flocculation [6], membrane separation [7], and adsorption [8–10]. Among the several techniques mentioned above, absorption methods are very proficient, economic, and widely used for wastewater treatment [11]. Nanostructures as a novel option for the removal of dyes offer a class of promising adsorbents that are ultra-fine and have a large surface area. Today, the use of adsorbents have been increased to remove the dyes from wastewater [12–18]. The shape of nanoparticles is a very important factor in determining their physical and chemical properties. For example, optical or catalytic properties [19], CdTe tetrapods [20], and Cu_2O coated with Cu nanoparticles [21] depend on their morphologies are different.

The structure of perovskites (ABO_3) is a combination of earth elements (A) and transition metals (B). By changing these elements, a wide range of these structures can be

* Corresponding author.

synthesized. The rare-earth ion at the A-site supplies the thermal resistance of perovskites and the transition metal cation at the B-site attributes mainly to the catalytic activity. $LaNiO_3$ perovskite has been used for many purposes such as electrode material, ferroelectrics because of its magnetic, and conductive thin films [22]. $LaNiO_3$ catalysts have been used for generating energy by producing a hydrogen-rich gas stream using ethane [23], methane [24], and glycerol steam reforming. The use of $LaNiO_3$ as a dye removal technique has been of great interest in recent years [25,26]. The main application of these nanoparticles includes the removable of methyl orange by $La_4Ni_3O_{10}$ [27], degradation of 4-chlorophenol in the La_2NiO_4 existence [27], Rhodamine B by $LaMO_3$ (M: Co, Cu, Fe, and Ni) [28], oxidation of phenol by using $LaBO_3$ (B: Cu, Fe, Mn, Co, Ni) [29], and decolorization of and removal of Reactive Black dye by $MoNiO_4$ perovskite [30].

The literature review on using perovskites in industrial pollutants shows that there are limited studies on pore size and perovskite surface area properties to remove the dyes. In the present study, molybdenum and nickel were used because of their high catalytic properties caused by their high vacancy orbital and an increase in their surface cavities by modifying them. Finally, to study the effect of increasing surface area on the dye adsorption, the dye adsorption in these two catalysts was studied. Therefore, in continuing our previous research on adsorption of dyes from aqueous solution [31–36], MNO and MNO modified with $Zn(NO_3)_2$ are synthesized and characterized and then a comparison is made between these two structures to adsorb Eriochrome Black T (EBT) dyes under different conditions such as contact time, pH, and adsorbent dosage. Finally, adsorption and kinetic isotherms are considered to obtain parameters effective in dye adsorption processes.

2. Materials and methods

Many materials including of citric acid (99% $C_6H_8O_7$, Merck, Darmstadt, Germany), ethylene glycol [99% $(C_2H_4(OH)_2$, Merck, Germany], nickel nitrate salt [99% $(Ni(NO_3)_2{\cdot}6H_2O$, Merck, Germany), molybdenum trioxide salt [MoO_3, 99%, Merck, Germany], zinc nitrate salt [$Zn(NO_3)_26H_2O$, 99%, Merck, Germany], and ammonium chloride (NH_4Cl, 99%, Merck, Germany) were used. The EBT, high quality, were prepared of Merck Company (Germany).

2.1. Instruments

Perovskite-structure, particle size, and phase purity of the samples were investigated by X-ray diffraction (XRD, Phillips PW 1840; k = 1.54056 Å). The peaks of the adsorbent diffraction pattern were typically scanned in the 2θ range of 10°–80° with a velocity of 1.5°min^{-1}. Fourier-transform infrared (FT-IR) spectra were measured on a Bruker (Germany) spectrophotometer pressed into KBr pellets and reported in wavenumbers (cm^{-1}). To measure nanoparticles size, a transmission electron microscopy (TEM, PHILIPS CM200 FEG apparatus, Netherlands) and a scanning electron microscope (SEM; Philips XL30, Netherlands) were used. UV-vis absorption spectra were prepared at 23°C–25°C temperature using a Cary 100 UV-vis spectrometer (Varian, USA). The Brunauer–Emmett–Teller (BET) method (Quantachrom CHEMBET-300, Austria) was used for evaluating the surface area.

2.2. Synthesis of MNO and MMNO perovskite structures

To synthesize the MNO compound, citric acid, distilled water, and nickel nitrate were added to a mixture of ethylene glycol under vigorous stirring. The molar ratio of citric acid to nickel nitrate was 5, and it was 1 for ethylene glycol to citric acid. After the nickel nitrate is completely dissolved, the MoO_3 was added to the stoichiometric ratio. The solution obtained at 60°C until a gel with high viscosity is mixed slowly by a magnetic stirrer, which may take 12–24 h. To calcinate the obtained gel, it was placed in an electric furnace at a temperature of 800°C for 4 h. The heating rate was 1°C min^{-1} up to 400 and 3°C min^{-1} up to 800°C [37,38]. The structure of the perovskite (MMNO) is based on a previous method [39]. In this method, Zinc nitrate was used to make holes on the perovskite MNO surface. In this experiment, the added $Zn(NO_3)_2$ in the final solution was transformed to ZnO with a perovskite structure. Then, to remove it, the ammonium chloride (2 M concentration) was required to dissolve and exit ZnO from the perovskite structure.

After etching this structure, it stayed in deionized water for 2 h. To stabilize the structure, after drying, the precipitate was re-calcined at 800°C. During the etching process, a small amount of ammonia was produced according to Eq. (1).

$$2NH_4Cl + ZnO \rightarrow 2NH_3 + ZnCl_2 + H_2O \quad (1)$$

The reason for using ZnO is its high ion radius, the formation of a hole in the perovskite structure, and easy dissolution and separation after its calcination.

2.3. Method

For the study, the adsorption ability of the EBT dye, several parameters were investigated such as pH, adsorbent dosage, temperature, and time. For adsorption experiments, the amount of 0.002–0.08 g of adsorbent was mixed with 10 mL EBT solution which preset pH, temperature, and dye concentration in a suitable amount. The pH value was adjusted between 2 and 11 using HCl (0.1 mol/L) or NaOH (0.1 mol/L) solution. Finally, using the spectrophotometer and the following equations were used to measure the amounts of adsorption and the adsorption capacity.

$$\%\text{Removal} = \frac{C_i - C_f}{C_i} \times 100 \quad (2)$$

$$q_e = \frac{(C_0 - C_e)V}{M} \quad (3)$$

where C_f is the initial and the C_i final concentrations of EBT in solution, q_e is the amount of absorption capacity, and the C_e and C_0, respectively, indicate a balanced and initial concentration of dye in solution (mg/L). Moreover, V and M, which indicate the solution volume (L) and dosage of the absorbance (g), respectively [40].

The kinetic models including pseudo-first-order and pseudo-second-order models and isotherms including Langmuir and Freundlich for EBT removal with adsorbents were applied to experimental data and adsorption parameters were calculated as reported in [16,34,41].

The PZC was calculated using the following method: First, to completely remove the CO_2 dissolved in the water, 100 mL of deionized water was added to an Erlenmeyer flask capped with cotton and then was heated for 20 min. Next, 10 mL of it was added into 25 mL Erlenmeyer flask with 0.5 g of adsorbent and mixed for 24 h at 25°C. Finally, the solution pH indicates the PZC. This method has shown satisfactory results elsewhere [42–44].

3. Results and discussion

3.1. Analysis of FT-IR, SEM analysis

Fig. 1 shows the FT-IR spectrum of the MNO and the MMNO. There are three peaks at 447, 629, and 960 cm^{-1} that related to the molybdenum and nickel bond in the structure. The peak at 3,436 cm^{-1} is related to the vibration of the OH groups in the structure of the $MoNiO_4$. After modification, the structure of the MMNO did not change and only a slight shift in the peaks occurred. Also, the peak at 3,444 cm^{-1} is related to stretching vibrations in O–H. Here, the peak intensity decreased for MMNO. The reason for the decrease in its intensity is the evaporation of the moisture in the structure of nanoparticles due to the increase in the number of cavities. As a result, these two structures are very similar to each other such that no changes are made by modifying the structure.

The images of TEM and SEM analysis related to the MMNO are shown in Fig. 2. From the SEM analysis, it can be concluded that the nanosized structure consists of spherical particles. Based on the results obtained from the TEM images, the MMNO particles are agglomerated and the diameter of the particles is 20–40 nm.

The findings of the XRD test for two samples of MNO and MMNO are presented in Fig. 3. Compared to standard cards, nanoparticles, or nano-adsorbents are well-synthesized because the sample peaks are like the standard sample $MoNiO_4$ (reference code: 98-003-6675). Also, the results show that the MNO structure has a perovskite crystal phase without any other crystalline phases by a relatively sharp peak. As mentioned before, to increase the $MoNiO_4$ surface area, etching operations using zinc nitrate were used. XRD patterns of the $MoNiO_4$ after etching, that is, MMNO, are presented in Fig. 3. After the etching operation, the original structure of $MoNiO_4$ is retained without the presence of zinc oxide in its structure.

Moreover, using the Scherrer equation, the average particle size is about 23.45 and 27.36 nm for MMNO and MNO, respectively.

3.2. Surface area and pore characteristics

Table 1 shows the results of the analysis of the surface area by BET method of MNO and MMNO perovskite catalysts.

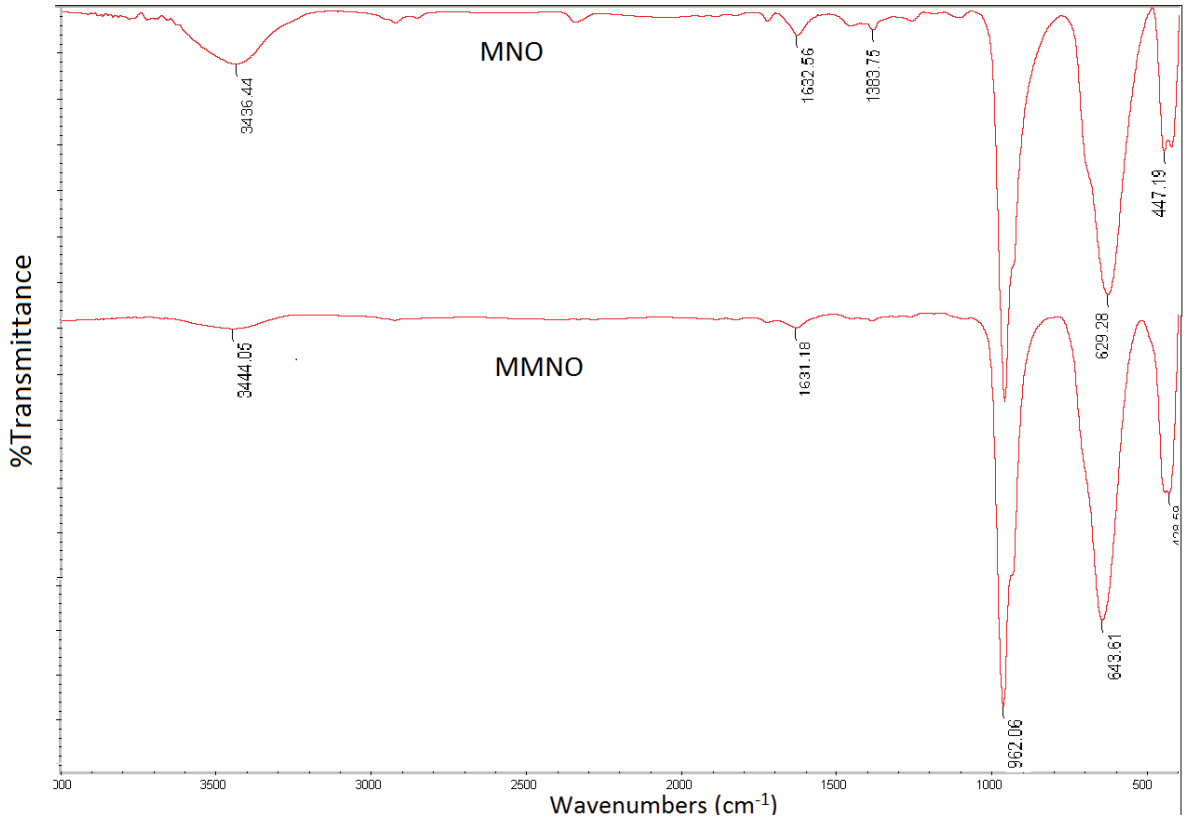

Fig. 1. FT-IR spectrum of MNO and MMNO perovskite surface.

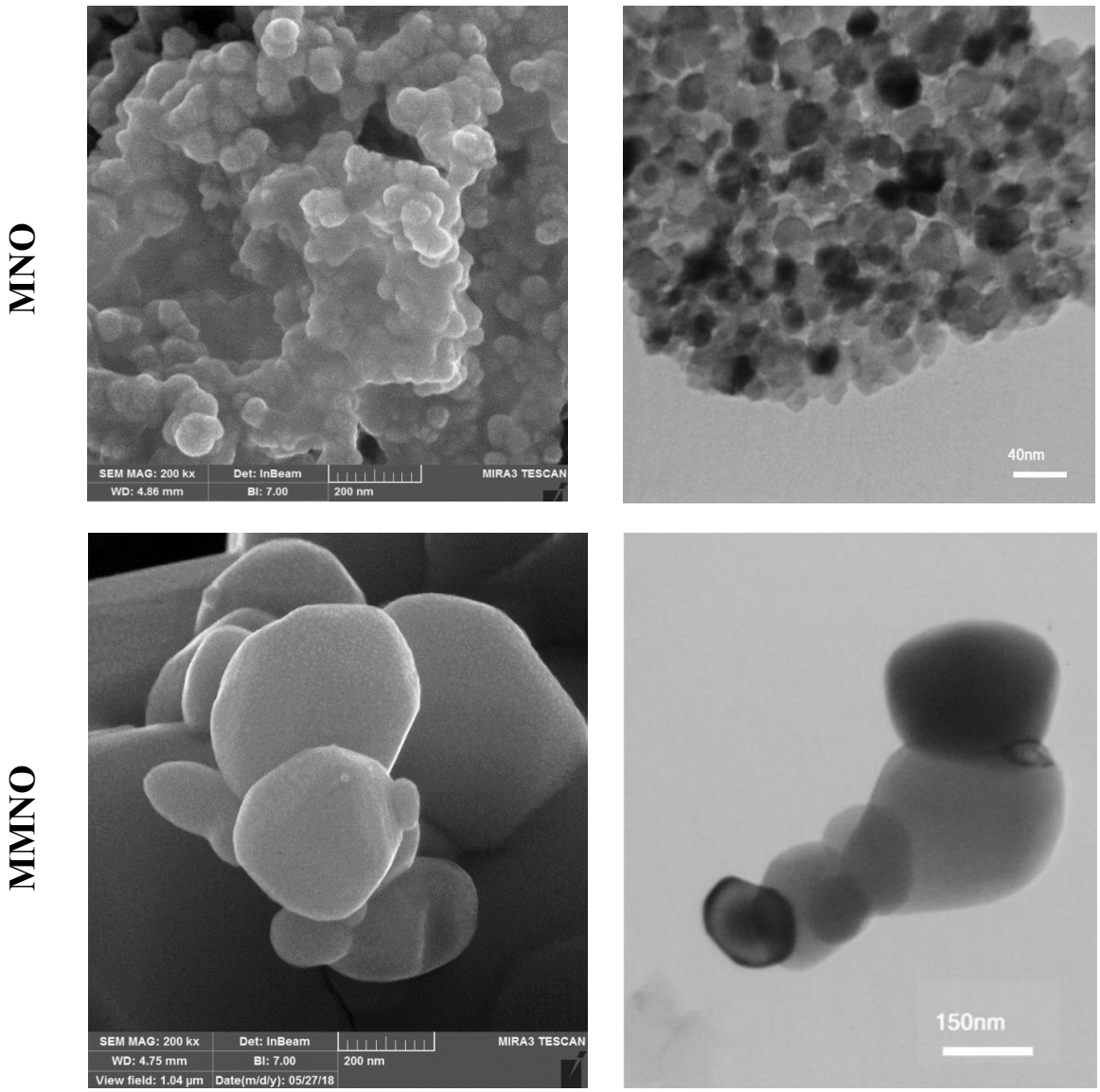

Fig. 2. TEM and SEM images of MNO and MMNO perovskite surfaces.

BET N_2 adsorption-desorption analysis was used to determine the specific surface area and pores size distribution in the MNO and MMNO nanostructures at 77 K (Fig. 4). The adsorption-desorption isotherms of MMNO sample did not have any hysteresis loop. However, for the MNO sample, it has a distinct H_3 hysteresis loop in the relative pressure (P/P_0) range of 0.55–1.0, indicating that the pore size distribution is not uniform [32]. The specific surface areas calculated for the MNO and MMNO based on the BET model are 2.83 and 3.03 $m^2\ g^{-1}$, respectively, and the pore volumes determined by the BJH approaches are 0.015 and 0.012 $cm^3\ g^{-1}$, respectively.

The special surface in the structure of MNO is less than that of the MMNO structure, which is synthesized by the sol–gel citrate method [39]. As can be seen, the mean pore diameters for MMNO and MNO are 15.378 and 21.576 nm, respectively. This reduction is due to zinc oxide created in the etching process in the final structure of the MMNO [39]. In the structure of MMNO, Zn has an effective atomic radius of 0.75 Å, which was replaced instead of the nickel element with an effective atomic radius of 0.6 Å. Moreover, this element provides a cavity in the final structure of MMNO.

3.3. Study of the operational parameters

One of the key factors in the general adsorption process is the effect of pH, which affects the chemical properties of both materials adsorbents and dyes in solution. To study the effect of pH on the adsorption process, 0.05g of adsorbent was added to 10 mL and 100 ppm of EBT solution, and the pH of the solution was set at 2–11. Fig. 5 demonstrates the dependence of pH on the EBT adsorption efficiency onto the adsorbents.

For the MNO and MMNO adsorbents, with increasing the pH, the removal amount of EBT is constant up to the pH of less than 7 and then decreases with increasing the pH

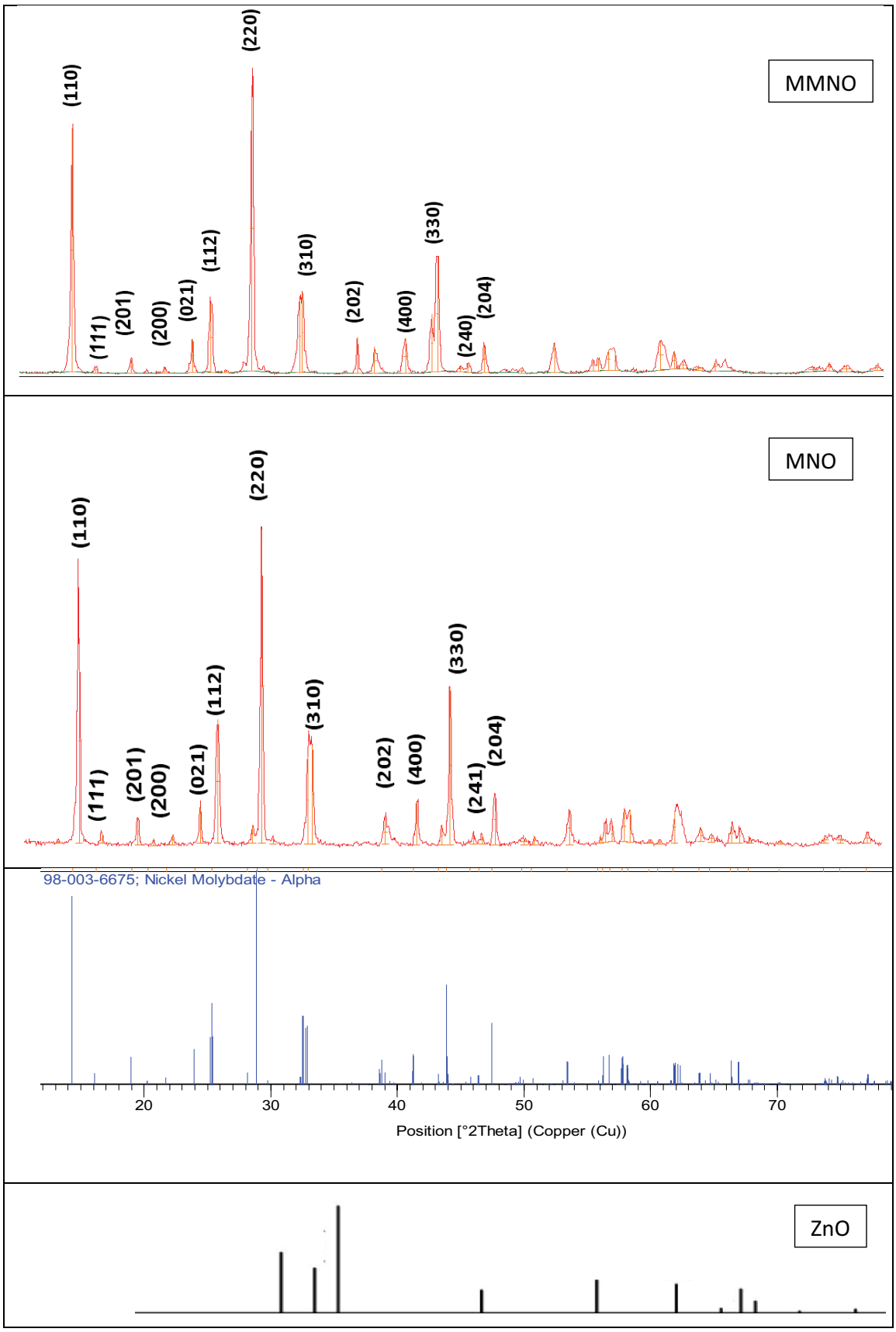

Fig. 3. Real and referenced XRD patterns of MNO samples after calcination at 800°C (reference code of $MoNiO_4$ sample: 98–003–6675).

Table 1
BET surface areas and crystallite size of MNO and MMNO samples

	MNO	MMNO
Surface area (m^2/g)	2.8328	3.0253
Mean pore diameter (nm)	21.576	15.378
Pore volume ($cm^3\ g^{-1}$)	0.015012	0.01211

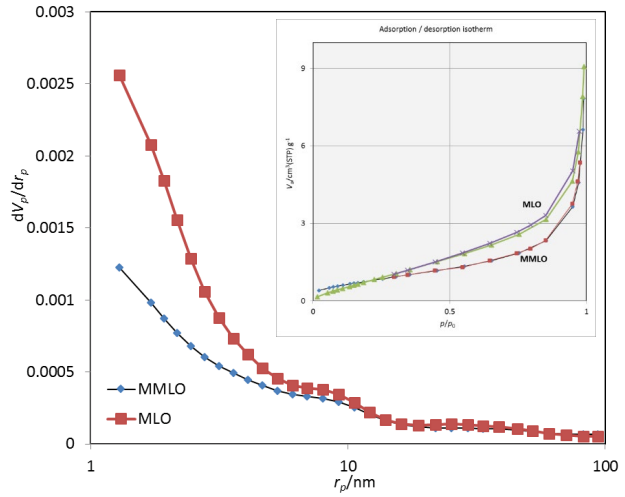

Fig. 4. Nitrogen adsorption–desorption isotherms and the corresponding pore size distribution curves for MNO and MMNO samples.

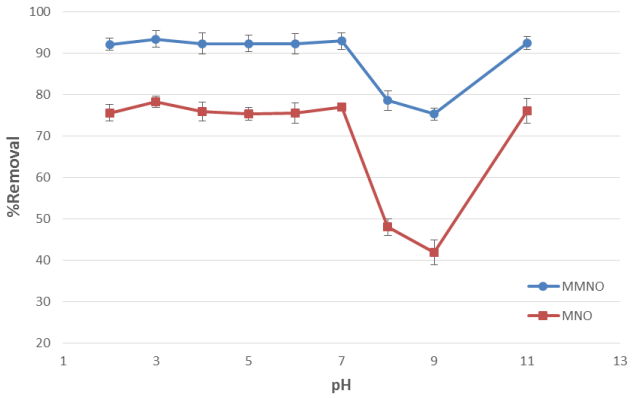

Fig. 5. Effect of pH on adsorption EBT dye on the adsorbents (conditions: 5 mg adsorbent, 10 mL of 100 mg/L of dye, duration of oscillation time of 30 min).

value. Thus, pH = 7 was selected as the best pH. The PZC values of the MNO and MMNO are 5.5 and 4.78, respectively. At lower pHs (pH < pH_{PZC}), the adsorbent had a positive charge. Moreover, EBT may be present in anionic forms. Under such conditions, EBT molecules have a high tendency to the absorbents. By increasing the pH value (pH ≥ pH_{PZC}), EBT removal tends to change in an inverse direction [45]. Since the adsorbent has a negative charge, there is a repulsion between dye and adsorbents.

However, as shown in Fig. 5, at pH = 11, the rate of absorption is increased probably due to degradation of the dye molecules by concentrated hydroxyls ions [41,46].

To study the effect of the adsorbent dosage on the dye removal, various dosages of the adsorbent for adsorption of the 100 ppm EBT solution were used. Results in Fig. 6 show that by increasing the adsorbent dosage of MNO from 0.002 to 0.08 g led to a decrease in the dye removal rate. The obtained optimal mass for the MNO adsorbent was equal to 0.05 g. Similar results were obtained for MMNO, where the optimal mass for the adsorbent was measured as 0.05 g.

With an increase in the amount of this adsorbent, the dye molecules are adsorbed more by these sites and thus trigger a jump in the amount of adsorption. In addition, according to Fig. 6, by increasing the amount of adsorbent, the amount of adsorption improves dramatically up to 0.05 g and then becomes more moderate.

As can be seen from Fig. 7, the removal efficiency increased with increasing the contact time and reached an optimum time at 25 min for adsorbents, and the removal percentage reached 77.2% and 96% for MNO and MMNO, respectively.

Afterward, the changes in adsorption increase were low. Therefore, because of the availability and abundance of vacant sites on the surface of the adsorbent, the rapid adsorption of EBT happens in the first few minutes.

3.4. Adsorption isotherms and kinetics

Fig. 8 presents the adsorption isotherm of adsorbents for EBT dye, which was fitted based on the adsorption process data. Table 2 shows the correlation coefficients and the adsorbent parameters. As can be seen from Table 2, the Langmuir model well fitted the adsorption isotherms and, theoretically, capacity absorption has the highest amount.

The EBT dye adsorption on the adsorbents occurred quickly, as is inferred from the values of $1/n$ and R_L obtained from the Langmuir and Freundlich models, respectively; however, the adsorption of dye occurred favorably. By considering the results of this section, it can be concluded that there is monolayer adsorption for the EBT dye on the adsorbents.

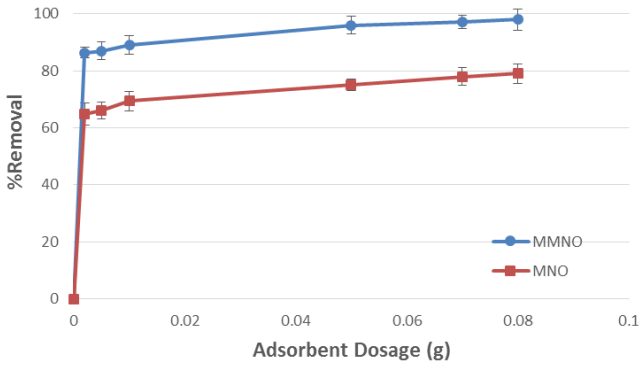

Fig. 6. Effect of adsorbent dosage on adsorption of dye on the adsorbents (conditions: 10 mL of 100 mg/L of EBT, duration of oscillation time of 30 min).

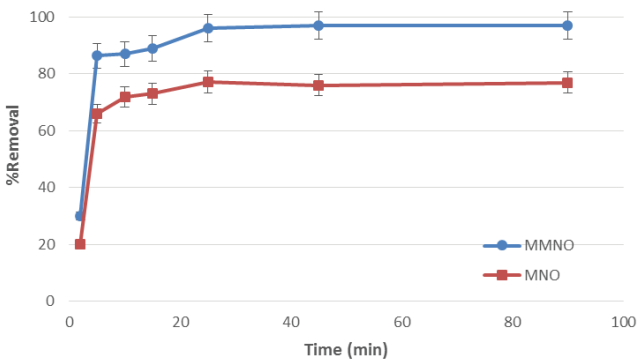

Fig. 7. Effect of reaction time on adsorption of EBT on the adsorbents (conditions: 10 mL of 100 mg/L of EBT).

Kinetic models can be used as an appropriate model for understanding the absorption mechanisms. The most widely used equations in this regard are the pseudo-first and second-order models. These two models were used to study the adsorption kinetics of the EBT dye by adsorbents.

According to Fig. 9, the pseudo-second-order model was fitted best to the experimental data, suggesting that the rate-limiting step is the chemical absorption that involves electron transfer between the absorbent and adsorbate by the valence force. The results of kinetic models are presented in Table 3.

3.5. Thermodynamic studies

The changes of enthalpy ($\Delta H°$), Gibb's free energy ($\Delta G°$), and entropy ($\Delta S°$) for the adsorption were determined by:

$$\ln K_l = \frac{\Delta S°}{R} - \frac{\Delta H°}{RT} \tag{4}$$

$$\Delta G° = \Delta H° - T\Delta S° \tag{5}$$

where T, R, and K_l are the solution temperature (K), universal gas constant (8.314, J K^{-1} mol^{-1}), and the equilibrium constant, respectively [47] and they are tabulated in Table 4.

The increased randomness at the solid/solution interface during the adsorption happens when the value of $\Delta S°$ is positive [48,49]. The positive values of $\Delta G°$ in Table 4 reveal that EBT dye adsorption on adsorbents is not spontaneous processes. Also, it is considered that the $\Delta G°$ values increased with increasing temperature from 20°C to 50°C, indicating that the method was more efficient at the lower temperature. Moreover, according to the Table 4 for dye adsorption by adsorbents, the negative value of $\Delta S°$ and positive value of $\Delta H°$ represents that the process is endothermic with decreasing in randomness at the solid-solution interface within adsorption [50]. The lower adsorption heat obtained for modified adsorbent indicated that physical rather than the chemisorption adsorption was prevailing [51].

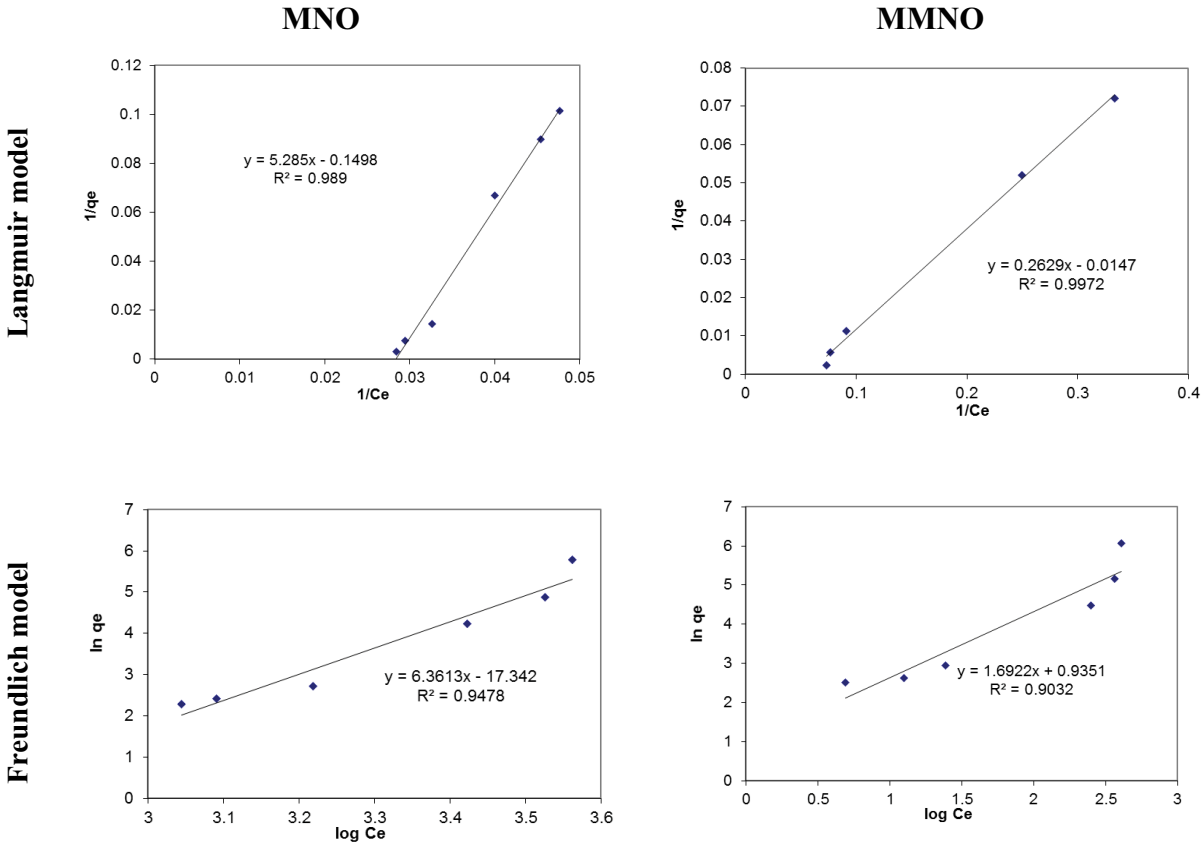

Fig. 8. Adsorption isotherms of dye adsorbed onto MNO and MMNO in aqueous solution; Langmuir model, and Freundlich model.

Table 2
Comparison of dyes adsorption capacity of different adsorbents

Adsorption isotherm		MMNO	MNO
Langmuir equation	R^2	**0.997**	**0.989**
	q_{max} (mg g^{-1})	**68.03**	**6.66**
	K_L (L mg^{-1})	0.056	0.0283
	R_L	0.151	0.260
Freundlich equation	R^2	**0.9032**	**0.948**
	K_F (mg g^{-1})	2.547	33,989,152.92
	$1/n$	0.591	0.157

3.6. Adsorption mechanism

To investigate the mechanism of EBT adsorption on adsorbents, the FT-IR spectra of EBT loaded adsorbents were used (Fig. 10). Comparing Fig. 10 with Fig. 2 reveals that no additional peak appears in the FT-IR analysis of structures after the end of the adsorption process. Results indicate that there is no interaction between the dye molecules and the adsorbent surface. Hence, it can be concluded that the mechanism of adsorption on the adsorbent is physical and the cause of the adhesion of dye to the adsorbent surface is the weak van der Waals forces.

Fig. 11 presents the structure and related properties of the EbT dye and adsorbent. The results show that adsorbent has many hydroxyl groups onto the surface; and a hydrogen bond will be formed by combining these groups with adsorbate and between them. Studying the dye reveals the sulfonyl group of EbT, with electron donor and receptor, is easy to combine with adsorbent and formed hydrogen bonds. The adsorption effect, in the EbT solution, mainly depends on hydrogen bonds. Because of the existence of electronic donors and receptors, the formation of the hydrogen bond is easy. Therefore, adsorbents of MNO and MMNO combine easily with many sulfonyl groups.

Also, the pore size and pore volume are important properties considered in the manufacture of materials as adsorbents for specific applications. They are accessible to a molecule of a given size. The physical adsorption mechanism in small pore size is mainly pore filling due to the overlapping of the pore; thus, larger molecules cannot access the small pore size of the adsorbent. Table 2 shows the maximum adsorption capacities of the MNO more than MMNO. It was 68.03 and 6.66 m^2/g for MMNO and MNO samples. The results of BET analysis (Table 1) also show that modifying the adsorbent increases very slightly in surface area and decreases the mean pore diameter. The mean pore diameters were 15.376 and 21.576 nm for MMNO and MNO samples, respectively.

It seems that the narrowing the pore size in the MMNO has led to an increase in the adsorption of the EBT molecules on the absorbent surface and increased the amount of adsorption capacity.

Based on BET results, it is seen that modification of the adsorbent surface, which increases the uniformity of pore size distribution, also rises dye adsorption. Shrinking the size of the cavities in the MMNO increased the catching of the EBT dye on the absorbent surface and increased the amount of dye adsorption.

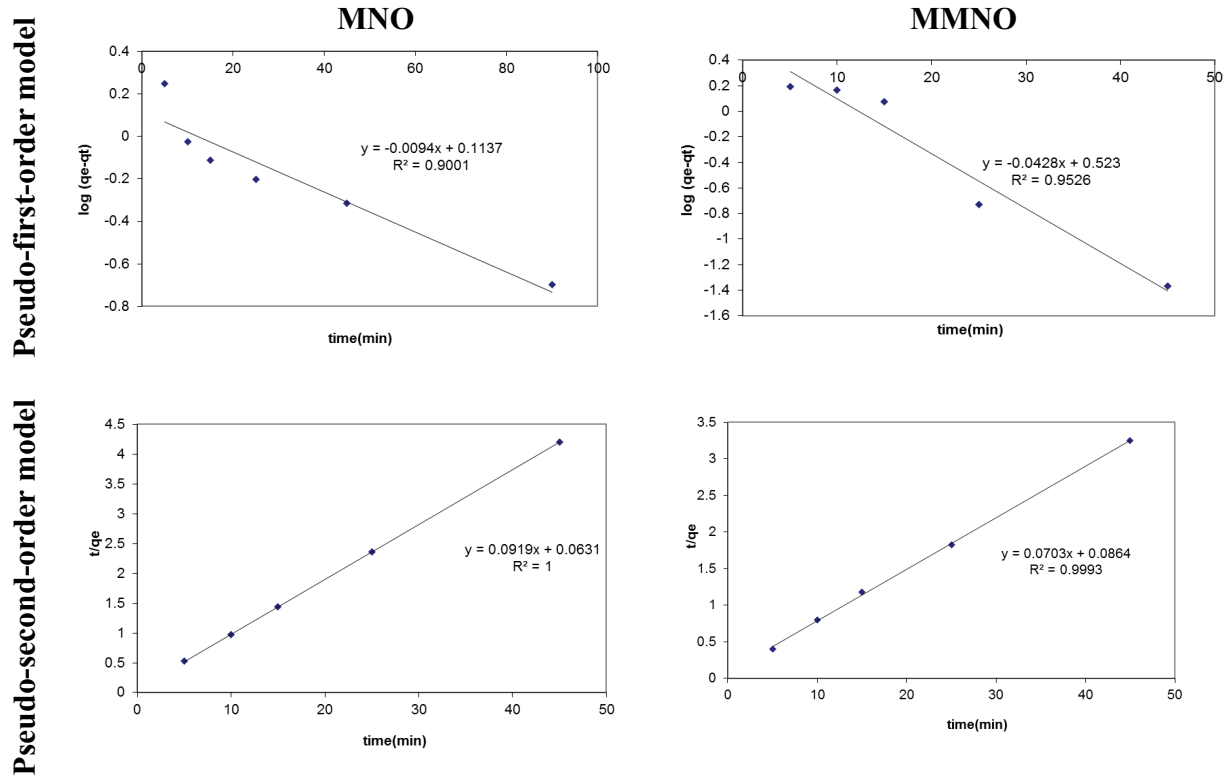

Fig. 9. Kinetic models for the adsorption of dyes; pseudo-first-order and pseudo-second-order kinetics.

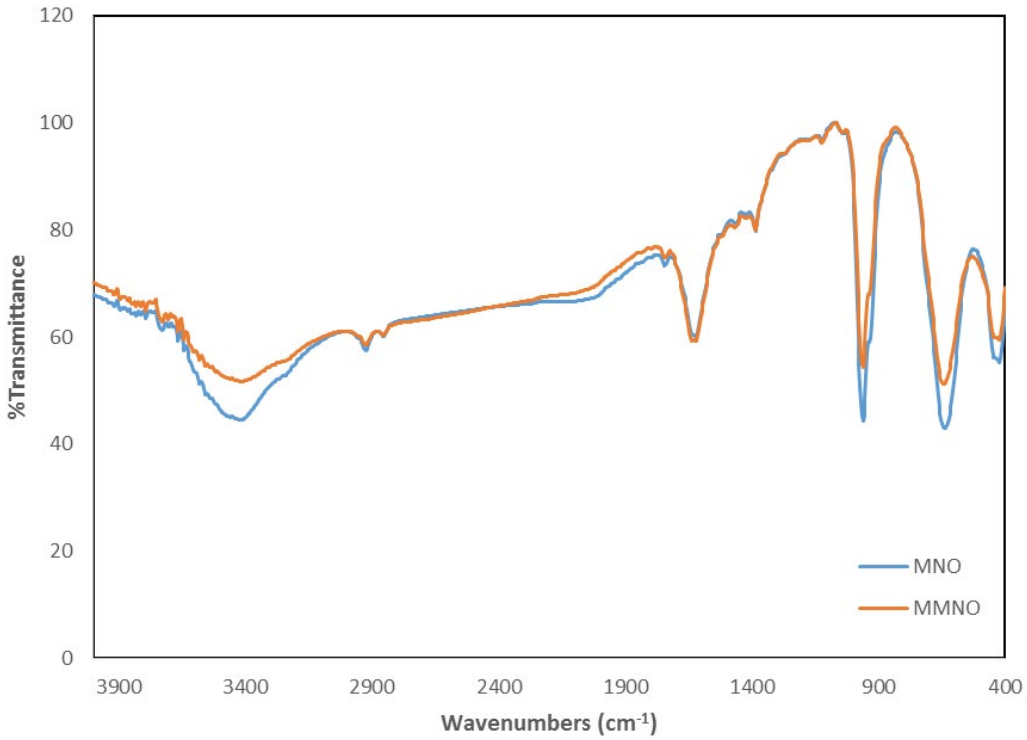

Fig. 10. Structures and properties of EBT dye and adsorbents.

Table 3
Pseudo-first-order model and pseudo-second-order model parameters constants for the adsorption of dyes on MMNO and MNO

Absorbents	Pseudo-first-order model			Pseudo-second-order model		
	k_1 (min^{-1})	q_e (mg g^{-1})	R^2	q_e (mg g^{-1})	k_2 (g mg^{-1} min^{-1})	R^2
MMNO	0.0428	3.33	0.953	14.22	0.0572	0.9993
MNO	0.0094	1.30	0.900	10.88	0.133	1

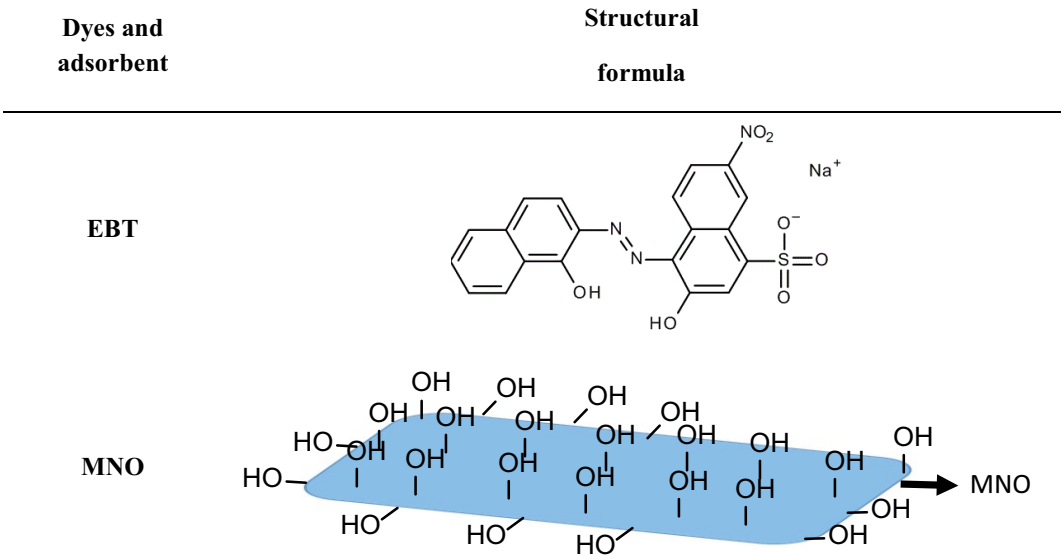

Fig. 11. FT-IR spectrum of MNO and MMNO perovskite surface after dye adsorption.

Table 5
Literature review on catalytic adsorption of dyes in the presence of various catalysts

Reference		[52]	[53]	[54]	[55]	[56]	[30]	This work	
Catalyst type		MoO_3	$CuO/\gamma\text{-}Al_2O_3$	Ni/MgAlO	$La_{0.8}K_{0.2}FeO_3$	Mo–Zn–Al, –O	$LaNiO_3$	$MoNiO_4$	Modified $MoNiO_4$
Dye		Rhodamine B	Methyl Orange, direct Brown, Direct Green 1,000	Basic Yellow 11	Methyl Blue	Cationic red GTL	Reactive Black 5	EBT	EBT
Operating condition	Initial dye concentration, mg/L	5	1,000	200	500	85	100	100	100
	Catalyst loading, g/L	0.5	27.71	4	1	2.72	1	5	5
	Temperature, °C	Room temperature	80	100	20–50	Room temperature	50	Room temperature	Room temperature
	pH	-	3	–	–	4	3	7	7
	Time, min	180	120	180	30	60	120	25	25
Dye removal efficiency		85.9%	99%	83%	~80%	80.1%	65.4%	73%	93%

Table 4
Thermodynamic parameters for the adsorption of adsorbents at different temperatures

			ΔΔ$G°$ (kJ/mol)		
			T (°C)		
	ΔΔ$S°$ (kJ/mol)	ΔΔ$H°$ (kJ/mol)	20	35	50
MMNO	–0.0267	1.195	9.89	10.34	10.78
MNO	–0.0403	3.140	14.94	15.54	16.15

Table 6
Adsorption capacity and parameters of EBT on other adsorbents

Adsorbent	pH	Time (min)	Isotherm/kinetic	q_m (mg/g)	References
Uncalcined-CoAl-LDH	2	120	Langmuir/second order	361.01	[57]
Bentonite-CoAl-LDH	2	120	Langmuir/second order	675.75	[57]
Activated carbon	2		Freundlich/second order	160	[58]
Graphene	2–4	120	Langmuir/second order	128	[59]
Maize stem	2		Langmuir/second order	167.84	[60]
Magnetite/pectin nanoparticles	2	60	Sip/second order	72.35	[61]
Cross-linked polyzwitterionic acid	3	30	Freundlich/second order	15.9	[62]
Calcined CoAl	2	60	Langmuir/second order	419.25	[63]
Modified $MoNiO_4$	7	25	Langmuir/second order	68.03	This work
$MoNiO_4$	7	25	Langmuir/second order	6.66	This work

3.7. Compare this research with previous research

Table 4 shows a comparison between previous research works, which have various transition metal-containing with this study [30,52–56]. Dye removal efficiencies using perovskite structure has been rarely reported in the literature. To the best of authors' knowledge, there is no study on the EBT removal in the presence of $MoNiO_4$ structure.

In various studies (Table 5), the initial concentration of dye is between 5 and 1,000 mg/L. Meanwhile, in the present research, 5 g/L of $MoNiO_4$ was removed from 100 mg/L dye solution because highly-concentrated dye solutions are more difficult to remove. For instance, 27.71 g/L of CuO/g-$_{Al_2O_3}$ was used for the treatment of 1,000 mg/L, 4 g/L of Ni/MgAlO for the treatment of 200 mg/L, and 27.71 g/L of CuO/g-Al_2O_3 for the treatment of 1,000 mg/L dye solutions [53,54].

To evaluate the practical applications of a system for removing the dye, the reaction time plays a very important role. Therefore, different times were investigated for up to 180 min. In the present study, the optimal time to remove dye by the $MoNiO_4$ structure at room temperature is 25 min. by reviewing the past papers in Table 5, it can be concluded that the $MoNiO_4$ structure has a high power of dyes removal at a better time.

The maximum adsorption capacities of EBT dye on other reported [57–63] adsorbents in the literature are presented in Table 6. The adsorption results confirmed that MMNO adsorbents exhibited higher adsorption capacity for dye, indicating a highly efficient and potential adsorbent for the treatment of anionic dye contaminated water.

4. Conclusion

In this study, the ability of EBT removal from aqueous solutions was examined by modified $MoNiO_4$ nanoparticles. Investigating the structure of the fabricated adsorbent was done using FT-IR, XRD, SEM, TEM, and BET analyses. We investigated the optimized conditions for studying the efficiency of $MoNiO_4$ structure as a compound for dye removal included $MoNiO_4$, reaction time, temperature, and pH of the solution. The significant results of this study are as follows:

- The optimum conditions for 100 mg/L EBT solution were pH of 7 and 5 g/L for adsorbents of MNO and MMNO, respectively.
- The adsorption capacity of EBT was obtained as 6.66 and 68.03 mg/g for MNO and MMNO, respectively.
- With increasing the dosage of MMNO, the adsorption amount decreased.
- Langmuir isotherm and pseudo-second-order model better predicted the adsorption isotherm and adsorption kinetics, respectively.
- Results of thermodynamic parameters indicated that the adsorption process was non-spontaneous and endothermic.

The results show that the structure of MMNO perovskite has high efficiency for the dye of EBT removal from industrial wastewater treatment.

References

[1] M. Stoyanova, I. Slavova, S. Christoskova, V. Ivanova, Catalytic performance of supported nanosized cobalt and iron–cobalt

mixed oxides on MgO in oxidative degradation of Acid Orange 7 azo dye with peroxymonosulfate, Appl. Catal., A, 476 (2014) 121–132.
[2] A. Ahmad, B. Hameed, Fixed-bed adsorption of reactive azo dye onto granular activated carbon prepared from waste, J. Hazard. Mater., 175 (2010) 298–303.
[3] Ö. Gerçel, H.F. Gerçel, A.S. Koparal, Ü.B. Öğütveren, Removal of disperse dye from aqueous solution by novel adsorbent prepared from biomass plant material, J. Hazard. Mater., 160 (2008) 668–674.
[4] P. Malik, S. Saha, Oxidation of direct dyes with hydrogen peroxide using ferrous ion as catalyst, Sep. Purif. Technol., 31 (2003) 241–250.
[5] M. Koch, A. Yediler, D. Lienert, G. Insel, A. Kettrup, Ozonation of hydrolyzed azo dye reactive yellow 84 (CI), Chemosphere, 46 (2002) 109–113.
[6] T. Panswad, S. Wongchaisuwan, Mechanisms of dye wastewater colour removal by magnesium carbonate-hydrated basic, Water Sci. Technol., 18 (1986) 139–144.
[7] G. Ciardelli, L. Corsi, M. Marcucci, Membrane separation for wastewater reuse in the textile industry, Resour. Conserv. Recycl., 31 (2001) 189–197.
[8] N. Thinakaran, P. Baskaralingam, M. Pulikesi, P. Panneerselvam, S. Sivanesan, Removal of Acid Violet 17 from aqueous solutions by adsorption onto activated carbon prepared from sunflower seed hull, J. Hazard. Mater., 151 (2008) 316–322.
[9] M. Anbia, S.E. Moradi, Adsorption of naphthalene-derived compounds from water by chemically oxidized nanoporous carbon, Chem. Eng. J., 148 (2009) 452–458.
[10] M. Anbia, K. Mohammadi, Novel and efficient nanoporous adsorbent for dichromate ion and furfural removal from aqueous solutions, Asian J. Chem., 21 (2009) 3347–3354.
[11] A. Namane, A. Mekarzia, K. Benrachedi, N. Belhaneche-Bensemra, A. Hellal, Determination of the adsorption capacity of activated carbon made from coffee grounds by chemical activation with $ZnCl_2$ and H_3PO_4, J. Hazard. Mater., 119 (2005) 189–194.
[12] A. Naghizadeh, M. Kamranifar, A.R. Yari, M.J. Mohammadi, Equilibrium and kinetics study of reactive dyes removal from aqueous solutions by bentonite nanoparticles, Desal. Water Treat., 97 (2017) 329–337.
[13] G. Zeydouni, M. Kianizadeh, Y. Omidi Khaniabadi, H. Nourmoradi, S. Esmaeili, M.J. Mohammadi, R. Rashidi, Eriochrme black-T removal from aqueous environment by surfactant modified clay: equilibrium, kinetic, isotherm, and thermodynamic studies, Toxin Rev., 38 (2018) 307–317.
[14] H. Rezaei, M.R. Narooie, R. Khosravi, M.J. Mohammadi, H. Sharafi, H. Biglari, Humic acid removal by electrocoagulation process from natural aqueous environments, Int. J. Electrochem. Sci., 13 (2018) 2379–2389.
[15] Y.O. Khaniabadi, H. Basiri, H. Nourmoradi, M.J. Mohammadi, A.R. Yari, S. Sadeghi, A. Amrane, Adsorption of Congo Red Dye from aqueous solutions by montmorillonite as a low-cost adsorbent, Int. J. Chem. React. Eng., 16 (2018) 1–11.
[16] F. Salimi, H. Rahimi, C. Karami, Removal of methylene blue from water solution by modified nanogoethite by Cu, Desal. Water Treat., 137 (2019) 334–344.
[17] P. Veerakumar, J. Tharini, M. Ramakrishnan, I. Panneer Muthuselvam, K.C. Lin, Graphene oxide nanosheets as an efficient and reusable sorbents for eosin yellow dye removal from aqueous solutions, ChemistrySelect, 2 (2017) 3598–3607.
[18] P. Veerakumar, T. Jeyapragasam, Surabhi, K. Salamalai, T. Maiyalagan, K.-C. Lin, Functionalized mesoporous carbon nanostructures for efficient removal of eriochrome black-T from aqueous solution, J. Chem. Eng. Data, 64 (2019) 1305–1321.
[19] R. Si, Y.W. Zhang, L.P. You, C.H. Yan, Rare-earth oxide nanopolyhedra, nanoplates, and nanodisks, Angew. Chem. Int. Ed., 117 (2005) 3320–3324.
[20] L. Manna, D.J. Milliron, A. Meisel, E.C. Scher, A.P. Alivisatos, Controlled growth of tetrapod-branched inorganic nanocrystals, Nat. Mater., 2 (2003) 382–385.
[21] S.U. Son, I.K. Park, J. Park, T. Hyeon, Synthesis of Cu_2O coated Cu nanoparticles and their successful applications to Ullmann-type amination coupling reactions of aryl chlorides, Chem. Commun., 7 (2004) 778–779.
[22] D. Aman, T. Zaki, S. Mikhail, S.A. Selim, Synthesis of a perovskite $LaNiO_3$ nanocatalyst at a low temperature using single reverse microemulsion, Catal. Today, 164 (2011) 209–213.
[23] A.L.A. Marinho, R.C. Rabelo-Neto, F.B. Noronha, L.V. Mattos, Steam reforming of ethanol over Ni-based catalysts obtained from $LaNiO_3$ and $LaNiO_3/CeSiO_2$ perovskite-type oxides for the production of hydrogen, Appl. Catal., A, 520 (2016) 53–64.
[24] A. Jahangiri, M. Saidi, F. Salimi, A. Mohammadi, Combined methane reforming over nano $LaNiO_3$ catalyst with modified active surface, Res. Chem. Intermed., 44 (2018) 1755–1773.
[25] Y. Li, S. Yao, W. Wen, L. Xue, Y. Yan, Sol–gel combustion synthesis and visible-light-driven photocatalytic property of perovskite $LaNiO_3$, J. Alloys Compd., 491 (2010) 560–564.
[26] W. Zhong, T. Jiang, Y. Dang, J. He, S.-Y. Chen, C.-H. Kuo, D. Kriz, Y. Meng, A.G. Meguerdichian, S.L. Suib, Mechanism studies on methyl orange dye degradation by perovskite-type $LaNiO_3$-δ under dark ambient conditions, Appl. Catal., A, 549 (2018) 302–309.
[27] J.-M. Wu, W. Wen, Catalyzed degradation of azo dyes under ambient conditions, Environ. Sci. Technol., 44 (2010) 9123–9127.
[28] K.-Y.A. Lin, Y.-C. Chen, Y.-F. Lin, $LaMO_3$ perovskites (M = Co, Cu, Fe and Ni) as heterogeneous catalysts for activating peroxymonosulfate in water, Chem. Eng. Sci., 160 (2017) 96–105.
[29] O.P. Taran, A.B. Ayusheev, O.L. Ogorodnikova, I.P. Prosvirin, L.A. Isupova, V.N. Parmon, Perovskite-like catalysts $LaBO_3$ (B = Cu, Fe, Mn, Co, Ni) for wet peroxide oxidation of phenol, Appl. Catal., B, 180 (2016) 86–93.
[30] B. Palas, G. Ersöz, S. Atalay, Catalytic wet air oxidation of Reactive Black 5 in the presence of $LaNiO_3$ perovskite catalyst as a green process for azo dye removal, Chemosphere, 209 (2018) 823–830.
[31] F. Salimi, M. Abdollahifar, P. Jafari, M. Hidaryan, A new approach to synthesis and growth of nanocrystalline AlOOH with high pore volume, J. Serb. Chem. Soc., 82 (2017) 203–213.
[32] F. Salimi, M. Abdollahifar, A.R. Karami, The effect of NaOH and KOH on the characterization of mesoporous AlOOH in the solvothermal route, Ceram. Silik., 60 (2016) 273–277.
[33] F. Salimi, S.S. Emami, C. Karami, Removal of methylene blue from water solution by modified nano-boehmite with Bismuth, Inorg. Nano Met. Chem., 48 (2018) 31–40.
[34] F. Salimi, M. Eskandari, C. Karami, Investigating of the methylene blue adsorption of wastewater using modified nano-zeolite by copper, Desal. Water Treat., 85 (2017) 206–214.
[35] F. Salimi, K. Tahmasobi, C. Karami, A. Jahangiri, Preparation of modified nano-SiO_2 by Bismuth and Iron as a novel Remover of Methylene blue from water solution, J. Mex. Chem. Soc., 61 (2017) 250–259.
[36] M. Mohamadi, F. Salimi, S. Sadeghi, Reduction of oil, COD and turbidity of Kermanshah oil refinery effluent using modified nano-zeolite by bismuth and iron, Desal. Water Treat., 97 (2017) 151–157.
[37] M. Goldwasser, M.E. Rivas, E. Pietri, M. Pérez-Zurita, M. Cubeiro, A. Grivobal-Constant, G. Leclercq, Perovskites as catalysts precursors: synthesis and characterization, J. Mol. Catal. A: Chem., 228 (2005) 325–331.
[38] L. Predoana, B. Malic, M. Kosec, M. Carata, M. Caldararu, M. Zaharescu, Characterization of $LaCoO_3$ powders obtained by water-based sol–gel method with citric acid, J. Eur. Ceram. Soc., 27 (2007) 4407–4411.
[39] J. Shu, S. Kaliaguine, Well-dispersed perovskite-type oxidation catalysts, Appl. Catal., B, 16 (1998) L303–L308.
[40] L. Cui, Y. Wang, L. Gao, L. Hu, L. Yan, Q. Wei, B. Du, EDTA functionalized magnetic graphene oxide for removal of Pb(II), Hg(II) and Cu(II) in water treatment: adsorption mechanism and separation property, Chem. Eng. J., 281 (2015) 1–10.
[41] J. Rezaee, F. Salimi, C. Karami, Removal of eriochrome black T dye from water solution using modified nano-boehmite by organic compounds, Desal. Water Treat., 139 (2019) 342–351.
[42] X. Deng, L. Lü, H. Li, F. Luo, The adsorption properties of Pb(II) and Cd(II) on functionalized graphene prepared by electrolysis method, J. Hazard. Mater., 183 (2010) 923–930.

[43] R. Leyva-Ramos, L. Bernal-Jacome, I. Acosta-Rodriguez, Adsorption of cadmium(II) from aqueous solution on natural and oxidized corncob, Sep. Purif. Technol., 45 (2005) 41–49.
[44] C. Moreno-Castilla, M.V. López-Ramón, F. Carrasco-Marín, Changes in surface chemistry of activated carbons by wet oxidation, Carbon, 38 (2000) 1995–2001.
[45] M. Heidari-Chaleshtori, A. Nezamzadeh-Ejhieh, Clinoptilolite nano-particles modified with aspartic acid for removal of Cu(II) from aqueous solutions: isotherms and kinetic aspects, New J. Chem., 39 (2015) 9396–9406.
[46] M. Kosmulski, pH-dependent surface charging and points of zero charge II. Update, J. Colloid Interface Sci., 275 (2004) 214–224.
[47] B.S. Inbaraj, J. Wang, J. Lu, F. Siao, B. Chen, Adsorption of toxic mercury (II) by an extracellular biopolymer poly (γ-glutamic acid), Bioresour. Technol., 100 (2009) 200–207.
[48] V.S. Mane, I.D. Mall, V.C. Srivastava, Kinetic and equilibrium isotherm studies for the adsorptive removal of Brilliant Green dye from aqueous solution by rice husk ash, J. Environ. Manage., 84 (2007) 390–400.
[49] P. Pimentel, M. Melo, D. Melo, A. Assuncao, D. Henrique, C. Silva, G. Gonzalez, Kinetics and thermodynamics of Cu(II) adsorption on oil shale wastes, Fuel Process. Technol., 89 (2008) 62–67.
[50] G. Sheng, J. Li, D. Shao, J. Hu, C. Chen, Y. Chen, X. Wang, Adsorption of copper(II) on multiwalled carbon nanotubes in the absence and presence of humic or fulvic acids, J. Hazard. Mater., 178 (2010) 333–340.
[51] G. McKay, Use of Adsorbents for the Removal of Pollutants from Wastewater, CRC Press, Boca Raton, 1995.
[52] J. Wang, S. Dong, C. Yu, X. Han, JJ. Guo, J. Sun, An efficient MoO_3 catalyst for in-practical degradation of dye wastewater under room conditions, Catal. Commun., 92 (2017) 100–104.
[53] L. Hua, H. Ma, L. Zhang, Degradation process analysis of the azo dyes by catalytic wet air oxidation with catalyst CuO/γ-Al2O_3, Chemosphere, 90 (2013) 143–149.
[54] G. Ovejero, A. Rodríguez, A. Vallet, J. García, Catalytic wet air oxidation of a non-azo dye with Ni/MgAlO catalyst, Chem. Eng. J., 215 (2013) 168–173.
[55] L. Zou, Q. Wang, Z. Wang, L. Jin, R. Liu, X. Shen, Rapid decolorization of methyl blue in aqueous solution by recyclable microchannel-like $La_{0.8}K_{0.2}FeO_3$ hollow microfibers, Ind. Eng. Chem. Res., 53 (2013) 658–663.
[56] Y. Xu, X. Li, X. Cheng, D. Sun, X. Wang, Degradation of cationic red GTL by catalytic wet air oxidation over Mo–Zn–Al–O catalyst under room temperature and atmospheric pressure, Environ. Sci. Technol., 46 (2012) 2856–2863.
[57] N.D. Mu'azu, N. Jarrah, T.S. Kazeem, M. Zubair, M. Al-Harthi, Bentonite-layered double hydroxide composite for enhanced aqueous adsorption of Eriochrome Black T, Appl. Clay Sci., 161 (2018) 23–34.
[58] M.D.G. de Luna, E.D. Flores, D.A.D. Genuino, C.M. Futalan, M.-W. Wan, Adsorption of Eriochrome Black T (EBT) dye using activated carbon prepared from waste rice hulls—optimization, isotherm and kinetic studies, J. Taiwan Inst. Chem. Eng., 44 (2013) 646–653.
[59] A. Khalid, M. Zubair, A comparative study on the adsorption of Eriochrome Black T dye from aqueous solution on graphene and acid-modified graphene, Arabian J. Sci. Eng., 43 (2018) 2167–2179.
[60] V.M. Vučurović, R.N. Razmovski, U.D. Miljić, V.S. Puškaš, Removal of cationic and anionic azo dyes from aqueous solutions by adsorption on maize stem tissue, J. Taiwan Inst. Chem. Eng., 45 (2014) 1700–1708.
[61] O.A. Attallah, M.A. Al-Ghobashy, M. Nebsen, M.Y. Salem, Removal of cationic and anionic dyes from aqueous solution with magnetite/pectin and magnetite/silica/pectin hybrid nanocomposites: kinetic, isotherm and mechanism analysis, RSC Adv., 6 (2016) 11461–11480.
[62] T.A. Saleh, A.M. Muhammad, S.A. Ali, Synthesis of hydrophobic cross-linked polyzwitterionic acid for simultaneous sorption of Eriochrome black T and chromium ions from binary hazardous waters, J. Colloid Interface Sci., 468 (2016) 324–333.
[63] M. Zubair, N. Jarrah, M.S. Manzar, M. Al-Harthi, M. Daud, N.D. Mu'azu, S.A. Haladu, Adsorption of eriochrome black T from aqueous phase on MgAl-, CoAl-and NiFe-calcined layered double hydroxides: kinetic, equilibrium and thermodynamic studies, J. Mol. Liq., 230 (2017) 344–352.